

Franck-Condon electron emission from polar semiconductor photocathodes

W. Andreas Schroeder¹, L. A. Angeloni¹, I-J. Shan¹, and L. B. Jones^{2,3}

¹ Department of Physics, University of Illinois Chicago, Chicago, IL 60607-7059, USA

² ASTeC, STFC Daresbury Laboratory, Warrington, WA4 4AD Cheshire, United Kingdom

³ Cockcroft Institute of Accelerator Science and Technology, Warrington, WA4 4AD Cheshire, United Kingdom

ABSTRACT. A presented analytical formulation of (optical)phonon-mediated and momentum-resonant Franck-Condon emission of photoexcited electrons from polar semiconductors is shown to be very consistent with (i) the observed emission properties of a Cesium-terminated GaAs(001) photocathode at 808nm [J. Phys. D: Appl. Phys. **54**, 205301 (2021)] and (ii) the measured spectral emission properties of a GaN(0001) photocathode from just below its bandgap energy to 5eV. The theoretical analysis in the parabolic band approximation predicts the form of both the quantum efficiency and mean transverse energy of photoemission as a function of the photocathode's electron affinity and the electron temperature in the vicinity of its emission face. The good agreement between theory and experimental data also suggests that sub-10nm rms surface roughness effects are not significant for polar semiconductor photocathodes.

Introduction

Semiconductor materials, particularly polar semiconductors [1], are fast becoming the photocathode material of choice for front-end photo-injectors [2-7] employed in XFELs [8] and potentially UED systems [9-13]. In large part this is because they offer enhanced performance over traditional metal photocathodes at more accessible visible to near UV wavelengths (i.e. photon energies $\hbar\omega$ less than 4eV) [14]. Quantum efficiencies (QEs) greater than 0.1% are routinely achieved for Cs₂Te [5,15-17], Cs₃Sb [18-22], and the bi-alkali photocathodes [2,23,24] due to their low electron affinity χ – the energy difference between the vacuum and the minimum of the semiconductor's conduction band into which electrons are photoexcited ($\chi = E_{\text{vac.}} - E_{\text{CBM}} = \phi - E_{\text{g}}$, where ϕ is the photoelectric work function measured from the valence band maximum and E_{g} is the semiconductor band gap). Single-crystal GaAs [25-28] and GaN (both wurtzite and zinc blende phases [29]), and III-V semiconductor strained superlattice heterostructures [30] have also been shown to allow spin-polarized electron beam generation – critical for studies of parity violation [31] and nucleon spin structure [32] and valuable for investigating magnetic properties and spin states in materials physics [33-35]. In these cases, Cesium-termination of the photocathode surface can generate a negative electron affinity (NEA) that leads to QEs well over 1% [36-44].

In contrast, measurements of the mean transverse energy (MTE) of the photoemitted electron distribution, defined using the rms transverse momentum (Δp_{T}) of the emitted electrons in the vacuum, $MTE = (\Delta p_{\text{T}})^2 / (2m_0)$, where m_0 is the free electron mass, have not generally conformed to

theoretical expectations for semiconductor photocathodes. Although in many cases the observed MTE approaches the thermal limit close to threshold [20,24,44], standard photoemission models [45-47] and Monte Carlo based simulations [48,49] of photoexcited electron emission (i.e., transport dynamics and emission physics with transverse momentum conservation [50]) predict lower values of the MTE, especially for GaAs [48,51], due to expected emission from a low effective mass conduction band [52-55]. As a result, surface roughness [56,57] (or scattering) effects are often invoked to explain the discrepancy [48,57-59], or alternatively an undefined mechanism that ensures electrons photoexcited into the conduction band(s) of the photocathode attain the free electron mass prior to emission [45,51].

In this Letter, we propose an alternative explanation for photo-excited electron emission from polar semiconductor photocathodes that is based on an (optical)phonon-mediated Franck-Condon (FC) scattering mechanism [59,60]. This momentum-resonant emission process has been observed directly in prior work by Rameau *et al.* [61] on a Hydrogen-terminated diamond(001) photocathode – a material with known strong optical deformation potential scattering [62]. Phonon scattering has also been invoked to explain inelastic electron emission [63] and the emitted electron energy distribution curves [64] from NEA GaAs and the emission properties of PbTe [65]. Our developed theoretical description of this emission process, based on the parabolic band approximation (as outlined in the Appendix), is shown to be in very good agreement with experimental measurements performed on Cesium-terminated *p*-type GaAs photocathodes for incident light at 808nm [44] and spectral characterization measurements performed on

a *p*-type GaN(0001) photocathode. These two photocathode studies represent the long and short electron transport length limits since, for incident photon energies close to but greater than their fundamental band gap, the absorption depth in GaAs [66] is an order of magnitude greater than that in GaN [67,68]. More specifically, the product of the absorption coefficient α and the electron drift velocity v_d towards the emitting photocathode face (due to internal and applied fields) is less than the optical phonon decay rate in GaAs, but greater in GaN, implying that the photoexcited electron distribution returns to the lattice temperature before emission in GaAs, but will need to equipartition its energy with the optical phonon modes in GaN [69].

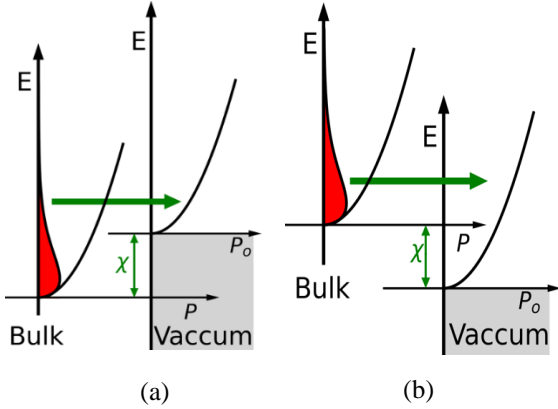


Figure 1

Schematic of Franck-Condon electron emission from a thermalized electron distribution in the parabolic band approximation for (a) positive electron affinity ($\chi > 0$) and (b) negative electron affinity ($\chi < 0$). A phonon of momentum \mathbf{q} facilitates a momentum-resonant electron transition (green arrow) from the bulk band states $E(p)$ to the vacuum states $E(p_0)$.

Franck-Condon Electron Emission

Our theoretical interpretation of momentum-resonant FC electron emission begins with the electron flux \mathbf{j}_e transmitted through the photocathode face into the vacuum. For a step work function potential barrier, it is straightforward to show that $j_z = p_{z0}/m_0$, under momentum resonant transmission over the barrier for which the barrier transmission probability $|T|^2 = 1$ (see the Appendix). As the transmitted vacuum electron momentum p_{z0} perpendicular to the photocathode face (the longitudinal z direction) can be written as $p_0 \cos \theta$, where θ is the polar angle, we obtain an angular emission dependence similar to that expected from surface roughness effects [57], and indeed from free-electron-like metal photocathodes [46]. The remaining analysis presented in the Appendix deals with the mapping of the photoexcited electron distribution in the photocathode band structure onto

the vacuum states under the momentum resonant assumption. For simplicity, only one isotropic parabolic emission band in the photocathode is considered for the cases of both positive and negative electron affinity χ (as shown in Figure 1) since this allows for an analytical solution. The resulting expressions for the QE and MTE associated with FC emission from a thermalized electron distribution at temperature T_e are

$$QE = A(k_B T_e)^2 [2k_B T_e + \chi] \exp\left[-\frac{\chi}{k_B T_e}\right] \quad 1(a)$$

$$MTE = k_B T_e \frac{[3k_B T_e + \chi]}{[2k_B T_e + \chi]} \quad 1(b)$$

for positive electron affinity (PEA) ($\chi > 0$) and

$$QE = A(k_B T_e)^2 [2k_B T_e + |\chi|] \quad 2(a)$$

$$MTE = \frac{|\chi|}{2} + k_B T_e \frac{[3k_B T_e + |\chi|]}{[2k_B T_e + |\chi|]} \quad 2(b)$$

for NEA ($\chi < 0$). In equations (1) and (2) k_B is Boltzmann's constant, and A is a constant that scales the QE due to various effects such as the details of the photoexcitation physics, carrier loss by recombination, etc. that are not included in the theoretical analysis. These expressions are shown below to well describe experimental measurements of the emission properties of studied Cesium GaAs [44] and bare GaN(0001) photocathodes. The presented formalism can also be readily extended using numerical techniques to emitting bands with more complex dispersion characteristics and emission from multiple bands.

Of immediate note is that for large PEA the MTE tends to a limiting value of $k_B T_e$ (equation 1(b)) and the QE falls as $\exp[-\chi/k_B T_e]$ (equation 1(a)) as should be expected for emission from the tail of a thermalized Boltzmann electron distribution. Further, at $\chi = 0$, the MTE = $\frac{3}{2}k_B T_e$ and the QE is simply proportional to $(k_B T_e)^3$, implying that lowering the electron temperature has a stronger adverse effect on the emission efficiency. And, for NEA, the MTE cannot be reduced below $\frac{1}{2}|\chi|$ (equation 2(b)) – an offset simply associated with the energy-conserving mapping of the emitting electron distribution onto the vacuum states (Figure 1(b)). In addition, it is important to note that the initial momentum of the electron in the emitting band state is not a factor because an intermediate particle (the optical phonon) is involved in the momentum-resonant FC emission process.

Although the FC analysis employs phonon scattering with a zero optical phonon energy (i.e., $\hbar\Omega = 0$), which

directly describes emission from the polaron (the quasi-particle generated by the coupling of conduction band electrons with ionic crystal vibrations [70,71]), it is readily modified for FC processes involving the emission of n phonons through a redefinition of the electron affinity; specifically, $\chi \rightarrow \chi + n\hbar\Omega$. The strength of the n^{th} FC emission process is given by Poisson statistics as $e^{-g}g^n/n!$ [72], where g is the dimensionless Fröhlich (or electron-(optical)phonon) coupling constant associated with optical deformation scattering [73]. For GaAs, $g = 0.068$ [71], so that over 93% of the emission occurs for $n = 0$ (i.e., direct emission from the polaron). On the other hand, for GaN ($g \approx 0.4$ [74]), the $n = 0, 1, 2, 3,$ and 4 emission modes are required to describe the FC emission process to an uncertainty of less than 0.1%. This means that an appropriately weighted sum is required to evaluate the total QE and hence also the MTE of electron emission. Fortunately, our analysis indicates that, to a very good approximation, the same results are obtained by evaluating equations (1) and (2) assuming that an average of g optical phonons are involved in the FC emission process; that is, by using an effective electron affinity of $\chi + g\hbar\Omega$. We note that this energy shift, $g\hbar\Omega$, is also equal to the real part of the electron self-energy shift above the (conduction) band minimum associated with the polaron quasi-particle [61,70]. This means that the $\hbar\Omega = 0$ analysis presented in the Appendix (i.e., χ evaluated using the energetic minimum of the emitting electronic band (Figure 1)) is an accurate approximation for (optical)phonon-mediated FC electron emission from semiconductor photocathodes.

Cesiated GaAs(001)

Figure 2 displays the measured QE and MTE (black data points) for a reflection-mode Cesiated p -type GaAs photocathode illuminated by 808nm light – a photon energy ($\hbar\omega = 1.53\text{eV}$) just above the 1.42eV band gap of the semiconductor where the absorption coefficient is $1.3 \times 10^4 \text{cm}^{-1}$ [66]. The semiconductor photocathode consists of a $2.4\mu\text{m}$ GaAs active layer with 10^{19}cm^{-3} Zn doping atop a $0.3\mu\text{m}$ $\text{Al}_{0.55}\text{Ga}_{0.45}\text{As}$ buffer layer grown on a n -type GaAs(001) substrate. The procedure used to obtain the experimental data is detailed in Refs. 44 and 75. Briefly, the QE and MTE are measured using the transverse energy spread spectrometer (TESS) photocathode characterization system equipped with laser light sources [76,77]. After an initial activation using a Cs-O yo-yo deposition, which produced an evaluated electron affinity of around -0.1eV , the photocathode's performance was monitored at 300K as a function of the electron affinity under its controlled degradation

(i.e., increase in electron affinity) through oxygen poisoning.

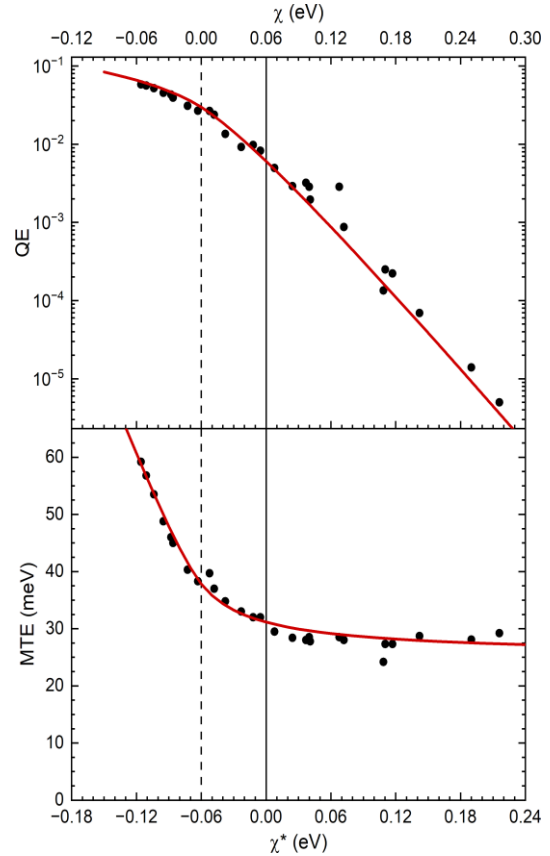


Figure 2

Experimental data (black points) and theoretical fits (red lines) for the QE (top panel) and MTE (bottom panel) as a function of the evaluated electron affinity χ^* (after Ref. 44) for a Cesiated p -type GaAs photocathode. The electron affinity $\chi = \chi^* + 60\text{meV}$ determined using the measured [44] and theoretical (see Appendix) longitudinal electron energy distribution curves is shown on the top axis and $\chi = 0$ by the vertical dashed line.

The displayed optimum fit (red lines in Figure 2) of the theoretical QE and MTE dependencies (equations (1) and (2)) to the experimental data require a 60meV shift towards negative electron affinity; in other words, $\chi^* = \chi - 60\text{meV}$. This shift is due to the difference in the definition of the electron affinity which for the presented theoretical FC emission model is defined as shown in Figure 1; that is, the energy difference between the minimum of the emitting bulk band and zero energy in the vacuum. In contrast, the plotted experimental value of the electron affinity, χ^* , was determined (with an estimated uncertainty of less than 13meV) by fitting the measured longitudinal emitted electron energy distribution to an expected functional form convolved with a 125meV FWHM

Gaussian instrument (resolution) function [44,75]. A direct comparison of the longitudinal energy distribution predicted by the FC emission mechanism (obtained by integration of the emitted electron distributions over the transverse momentum p_T , as described in the Appendix) and their measurement [44] indicates that the TESS instrument resolution is closer to 10meV rather than 125meV, and so the latter is the major contributing factor to the 60meV difference between χ^* and χ . Both theoretical fits to the experimental QE and MTE data employ $k_B T_e = 27\text{meV}$ (i.e., an electron temperature just above 300K) – the limiting value of the MTE for large PEA (bottom panel of Figure 2 and equation 1(b)). This is to be expected since the long $\sim 1\mu\text{m}$ absorption depth (i.e., transport length) in GaAs at 808nm provides the photoexcited electron distribution in the conduction band sufficient time for optical phonon emission to cool to near the lattice temperature while internal and applied fields accelerate the electrons towards the emission face. The analysis presented in Ref. 73 for this equilibrium case of electron drift with $T_e/T = 1.06$, where T is the 300K lattice temperature, indicates $\mu_e E_{av} \approx 0.25v_{ds}$, where μ_e is the electron mobility, E_{av} is the average acceleration field experienced by the electrons, and v_{ds} is their saturation drift velocity. For GaAs (optical phonon energy $\hbar\Omega \approx 36\text{meV}$ and conduction band effective mass $m^* = 0.067m_0$), $v_{ds} \approx \sqrt{3\hbar\Omega/(4m^* \coth(\hbar\Omega/2T))} = 2.1 \times 10^5\text{m/s}$ [73] and $\mu_e \approx 1,600\text{cm}^2/(\text{V}\cdot\text{s})$ for the 10^{19}cm^{-3} dopant density [79], implying that $E_{av} \sim 3\text{kV/cm}$. This value for the average acceleration field is somewhat short of the expected $\sim 100\text{MV/m}$ surface depletion field of the p -type GaAs photocathode (assuming $\sim 0.5\text{eV}$ band bending [79]) and so suggests that either (i) the Cesium of the surface significantly reduces the band bending (through the introduction of new surface states) or (ii) the majority of the emitted electrons originate from bulk states beyond the $\sim 10\text{nm}$ surface depletion region. The latter is quite likely since the transport analysis in Ref. 73 also indicates that the electrons drift with a velocity of $\mu_e E_{av} \approx 0.25v_{ds} = 5 \times 10^4\text{m/s}$ and hence, including the acceleration due to the internal fields, the time for an electron to transit the depletion region is somewhat less than the characteristic $\sim 200\text{fs}$ optical phonon emission time in GaAs [73,80].

GaN(0001)

In contrast to the GaAs photocathode, the emission surface of the studied p -type wurtzite GaN(0001) photocathode from Kyma Technologies Inc. [81] is not Cesium. The photocathode is fabricated using hydride vapor-phase epitaxy (HVPE) techniques on a sapphire substrate and consists of a $1\mu\text{m}$ -thick ‘active’

layer with $5 \times 10^{17}\text{cm}^{-3}$ Mg doping grown atop a $2\mu\text{m}$ buffer layer of undoped GaN. The epi quality (sub-1nm rms surface roughness) GaN(0001) surface is N-polar terminated due to the growth orientation of the sapphire substrate [82,83] for which in-house DFT-based thin-slab calculations of the work function [84] indicate a value of $5.8(\pm 0.2)\text{eV}$ as measured from the valence band maximum – a value that is consistent with prior work [85]. For the 3.4eV band gap of GaN at 300K [86], this implies that the conduction band minimum (CBM) has a PEA of about 2.4eV which will severely limit emission of near room temperature electrons as the Boltzmann factor $\exp[-E/k_B T] \sim 10^{-41}$. On the other hand, the band structure of wurtzite GaN [87] also indicates the presence of an upper conduction band $\sim 2.5\text{eV}$ above the CBM which, if populated, would allow more efficient and likely NEA electron emission.

Surface band bending due to the p -type Mg doping of the GaN semiconductor generates a depletion region with a $\sim 40\text{nm}$ depth (assuming $1.0\text{--}1.8\text{eV}$ of band bending [88]) which is of the same order as the $50\text{--}100\text{nm}$ absorption depth for incident photon energies just above the 3.4eV band gap [86]. For the resultant average depletion field of $\sim 10\text{MV/m}$, the room temperature electron drift velocity is $1\text{--}2 \times 10^5\text{m/s}$ [86,89-91] (and likely higher for hot photoexcited electrons), giving a transit time over the depletion region significantly less than 1ps ; that is, less than the expected $\sim 1\text{ps}$ optical phonon decay time at our $5 \times 10^{17}\text{cm}^{-3}$ dopant density [92]. This means that electrons photoexcited into the conduction band with an excess energy ΔE (with respect to the CBM) will initially (on a sub-100fs timescale within the $\sim 0.5\text{ps}$ incident laser pulse duration) equipartition their energy with the $l = 6$ primary Γ -point optical phonon modes in GaN [93] and this equipartitioned energy should be maintained during electron emission as they drift to the GaN(0001) photocathode face. The electron temperature T_e of the emitting electron distribution for an incident photon energy $\hbar\omega$ is then given by

$$k_B T_e = \frac{2\Delta E}{3(l+1)} = \frac{2\mu(\hbar\omega - E_g)}{3m_e(l+1)} \approx \frac{1}{12}(\hbar\omega - E_g) \quad (3)$$

in the parabolic band approximation, where $m_e = 0.22m_0$ and $m_h \approx 1.25m_0$ are the effective masses of the conduction band [86,89] and valence band (heavy hole) [95] states near the Γ point, respectively, and the reduced mass $\mu = m_e m_h / (m_e + m_h)$.

Figure 3 displays the measured spectral dependence of the MTE and QE for the p -type GaN(0001) photocathode at 300K. The experimental data was

obtained using the sub-picosecond tunable UV laser and the 10-20kV DC gun-based photocathode characterization system described in Refs. 95 and 96. As expected, the QE (top panel of Figure 3) shows an onset at around the 3.4eV band gap energy and is overall much smaller than that measured for the Cesium GaAs photocathode (Figure 2) due to the $\sim 2.4\text{eV}$ PEA of the CBM. Also noticeable is a non-zero QE below the band gap energy which we ascribe to photoexcitation into the conduction band from the Mg dopant states [29] 100-200meV above the valence band maximum [97]. These low excess energy photoexcited electrons are generated throughout the $1\mu\text{m}$ -thick p -doped GaN region due to the low (less than 10^4cm^{-1}) absorption coefficient in this spectral region. This means that below $\hbar\omega \approx 3.4\text{eV}$ the photoexcited electrons will drift into the surface depletion region at close to room temperature (as was the case for the GaAs photocathode irradiated at 808nm), but then undergo acceleration in the dominant internal field of the $\sim 40\text{nm}$ surface depletion region. For the average $\sim 10\text{MV/m}$ depletion field strength and the expected $\sim 400\text{cm}^2/\text{V}\cdot\text{s}$ electron mobility at the $5 \times 10^{17}\text{cm}^{-3}$ dopant density [98], the transport analysis in Ref. 73 indicates that an electron temperature close to the 880K Debye temperature T_D of GaN [99] should be attained (i.e., $k_B T_e \approx k_B T_D = 75\text{meV}$), leading to the sub-bandgap MTE signals in Figure 3. We note here that the $\sim 3\text{nm}$ product of the characteristic $\sim 20\text{fs}$ optical phonon scattering time in GaN [73,100] with the $1.2 \times 10^5\text{m/s}$ electron drift velocity [86,89-91] is much less than the $\sim 40\text{nm}$ width of the surface depletion region, thus ensuring that a thermalized electron distribution is maintained.

For incident photon energies greater than the $E_g \approx 3.4\text{eV}$ band gap, band-to-band absorption dominates driving the photocathode's electron emission dynamics into the short transport length regime where $k_B T_e$ is dependent upon $\hbar\omega - E_g$ (equation 3). Indeed, the red line in the bottom panel of Figure 3 employs $k_B T_e = k_B T_D + \frac{1}{12}(\hbar\omega - E_g)$ for $E_g > 3.3\text{eV}$ and $\chi \approx -0.3\text{eV}$ to fit the experimental MTE data using equation (2b). The latter negative value for the electron affinity, which is required to describe the 230meV offset in the measured MTE at $\hbar\omega \approx E_g$, confirms that the observed emission originates from electrons in the upper conduction band 2.5eV above the CBM in GaN. For the downward $\sim 1\text{eV}$ band bending [88] and our calculated intrinsic $\chi = -0.1(\pm 0.2)\text{eV}$ for the upper conduction band, this value of an 'effective' electron affinity for the FC emission process suggests that only electrons well within the photocathode's $\sim 40\text{nm}$ surface depletion region are emitted through the optical phonon

scattering mechanism. In fact, assuming parabolic band bending towards the p -type GaN(0001) surface, a 0.2eV band energy increase (about one fifth of the band bending) is achieved $\sim 5\text{nm}$ from the surface – a distance corresponding to ~ 10 lattice constants that may reflect the spatial overlap required in GaN between the bulk and emitted vacuum electron wavefunctions plus that of the scattering optical phonon (i.e., lattice vibration) for the FC emission process.

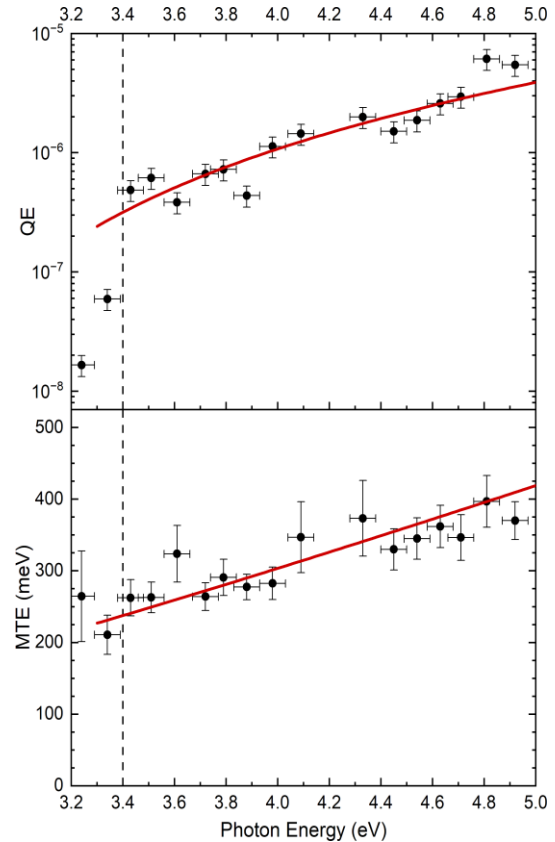


Figure 3

Experimental data (black points) and theoretical fits (red lines) for the QE (top panel) and MTE (bottom panel) as a function of the incident photon energy for the p -type GaN(0001) photocathode. The 3.4eV bandgap of GaN is indicated by the vertical black dashed lines.

Using equation (2a), the measured spectral variation of the QE is also consistent with a NEA of 0.3eV and the same $k_B T_e$ dependence on $\hbar\omega$ used to fit the MTE data as illustrated by the red line fit in the top panel of Figure 3. Further, the $\sim 10^{-6}$ QE observed over most of the investigated spectral range is quite consistent with the average 100-150meV electron energy $k_B T_e$ due to the $\exp[-E/k_B T_e] \sim 10^{-8}$ Boltzmann factor and the estimated factor of 100 difference in the density of states between the upper and lower conduction bands.

Summary

An analytical theoretical formulation of (optical)phonon-mediated FC electron emission for polar semiconductor photocathodes is presented that accurately describes the measured spectral emission properties of a p -type GaN(0001) photocathode and those at 808nm of a Cesiumated p -type GaAs photocathode as its electron affinity is degraded (i.e., increased) by controlled oxidation at 300K [44]. Specifically, experimental QE and MTE data obtained for both photocathodes are fit using the FC emission theory presented in the Appendix with electron temperatures of $k_B T_e = 27\text{meV}$ for GaAs and $k_B T_e = k_B T_D + \frac{1}{12}(\hbar\omega - E_g)$ when $\hbar\omega > 3.3\text{eV}$ for GaN – the values expected for their long and short transport length regimes respectively. Further, the surface roughness of the two photocathodes is somewhat different; the (0001) GaN surface is of epi polished quality with a sub-1nm rms surface roughness whereas the (001) GaAs photocathode surface is somewhat rougher due to the Cesiumation and subsequent oxidation with a rms surface roughness of 2-6nm being reported [101-103]. Consequently, the clear implication is that sub-10nm rms surface roughness does not play a major role in electron emission from polar semiconductors – a conclusion consistent with a recent multi-dimensional analysis of the effects of surface roughness [104]. Further, a FC electron emission process should not be strongly affected by surface roughness effects since it is energy and momentum resonant; that is, an electron can only be emitted into the vacuum if the scattering process in the solid-state photocathode produces an electronic state that satisfies $E = p^2/(2m_0)$ with a positive z -component (longitudinal) momentum for any polar (θ) emission angle.

The presented momentum-resonant FC process is expected to dominate the electron emission of all solid-state photocathodes with sufficiently strong optical deformation potential scattering; the Fröhlich coupling constant g for GaAs is only 0.068 [71], whereas that for both diamond ($g = 1.1$ [61]) and GaN ($g \approx 0.4$ [74]) are much larger. Highly polar semiconductor photocathode materials like Cs_2Te , Cs_3Sb , and the bi-alkali antimonides should certainly exhibit dominant electron emission due to the (optical)phonon-mediated FC mechanism. We note, for example, that the limiting (near threshold) value of the 300K MTE measured for Cs_3Sb at 690nm ($\hbar\omega = 1.797\text{eV}$) is 35-40meV [20] rather than 25meV. Recent *ab initio* band structure calculations for cubic Cs_3Sb [105] indicate that this could be expected for $k_B T_e \approx 25\text{meV}$ (the long transport length limit): An upper conduction band exists near the vacuum level at

0.4-0.5eV above its CBM giving $\chi \approx 0$ for emission from this band (as Cs_3Sb has a PEA of around 0.45eV [18]) so that equations 1(b) and 2(b) for the FC emission mechanism predict $MTE \approx \frac{3}{2} k_B T_e = 38\text{meV}$. Notably, this 300K MTE measurement for p -type Cs_3Sb has also been attributed, using Monte Carlo modeling techniques, to photoexcitation into the conduction band from excess Sb acceptor states $\sim 0.4\text{eV}$ above the valence band and subsequent electron emission that does not conserve transverse momentum [106]. Clearly, the former is energetically equivalent to the upper conduction band from band structure calculations while the latter is a partial physical representation of the FC emission process presented here.

Acknowledgements

This work was supported by the U.S. Department of Energy under Award no. DE-SC0020387 and part-funded by UKRI-STFC through the ASTeC core grant. The authors are also indebted to H.E. Scheibler for sharing access to experimental data from Ref. 44 and clarifying the analysis methods employed.

Appendix

Within the parabolic band approximation, an analytical expression for momentum-resonant Franck-Condon (FC) electron emission mediated by optical phonon scattering can be derived. For the case of a step potential photoemission barrier, the over-barrier transmitted electron flux \mathbf{j}_z in the longitudinal (z) direction perpendicular to the photocathode surface may be expressed as

$$j_z = \frac{p_{0z}}{m_0} |T|^2 = \frac{p_z}{m^*} (1 - |R|^2) = \frac{4p_{0z}p_z^2}{m^*(p_{0z} + p_z)^2}$$

where the emission is from a bulk band with an energy dispersion $E = \frac{p^2}{2m^*}$ to a vacuum band with $E_0 = \frac{p_0^2}{2m_0}$ (m^* is the effective mass of the electron-like bulk band, m_0 is the free electron mass, p is the electron momentum in the emitting band, and p_0 is the emitted electron momentum in the vacuum), and $|T|^2$ and $|R|^2$ are the usual transmission and reflection probabilities for the square barrier. For momentum-resonant emission, $p_z = p_{0z}$, so that the transmitted electron flux simply becomes

$$j_z = \frac{p_{0z}}{m^*} = \frac{p_0 \cos\theta}{m^*}$$

where θ is the polar emission angle. This angle and momentum dependence for the transmitted electron flux is incorporated in the following analysis of FC electron emission for the simplified case where the

energy of the mediating (optical) phonon $\hbar\Omega$ is taken to be zero; that is, much smaller than the characteristic energy of the electron distribution $k_B T_e$, where k_B is Boltzmann's constant and T_e is the electron temperature. As a result, the mathematical description of the emission process becomes a straightforward energy-conserving mapping of the electron distribution in the emitting bulk band states that are above the vacuum level onto the vacuum density of states (DOS), as any vacuum state may be populated through the momentum-resonant FC emission mechanism. Positive ($\chi > 0$) and negative ($\chi < 0$) electron affinity cases for the emitting band are considered separately and the derived expressions for the MTE and QE collapse to the same value for zero electron affinity, i.e., $\chi = 0$.

i) Positive Electron Affinity

For the case of positive electron affinity (PEA), where the minimum of the emitting band is below the vacuum level, so that $E = E_0 + \chi$, the momentum-space energy mapping requires

$$p^2 = \left(\frac{m^*}{m_0}\right) p_0^2 + 2m^* \chi$$

which allows a three-dimensional non-degenerate electron distribution from E to $E + dE$ in the emitting bulk band, namely $\sqrt{E} \cdot \exp[-E/(k_B T_e)]$, to be written in the vacuum momentum space as $\left\{\left(\frac{m^*}{m_0}\right) p_0^2 + 2m^* \chi\right\} \exp\left[-\frac{p_0^2}{2m_0 k_B T_e} - \frac{\chi}{k_B T_e}\right]$ for the interval p_0 to $p_0 + dp_0$. Integration in spherical co-ordinates over the positive p_{z0} momentum half-space in the vacuum DOS with the flux transmission dependence then gives the number of emitted electrons N ;

$$\begin{aligned} N &= 2\pi A \int_0^{\frac{\pi}{2}} d\theta \sin\theta \cos\theta \int_0^\infty dp_0 p_0^2 \left(\frac{p_0}{m^*}\right) \left\{\left(\frac{m^*}{m_0}\right) p_0^2 + 2m^* \chi\right\} \exp\left[-\frac{p_0^2}{2m_0 k_B T_e} - \frac{\chi}{k_B T_e}\right] \\ &= \pi A (2m_0 k_B T_e)^2 [2k_B T_e + \chi] \exp\left[-\frac{\chi}{k_B T_e}\right] \end{aligned}$$

where the integration over the azimuthal angle ϕ has been performed and A is a constant containing all effects not associated with the emission physics: dimensional constants for the vacuum DOS, spin degeneracy, carrier recombination, etc. The above expression therefore provides the expected dependence of the barrier emission QE on T_e and χ for the PEA FC process; in other words

$$QE \propto (k_B T_e)^2 [2k_B T_e + \chi] \exp\left[-\frac{\chi}{k_B T_e}\right]$$

The MTE of the emitted electrons can now be evaluated using the suitably normalized expectation value $\langle \frac{p_0^2}{2m_0} \rangle = \langle \frac{p_0^2 \sin^2\theta}{2m_0} \rangle$, where p_T is the transverse electron momentum, viz;

$$\begin{aligned} MTE &= \frac{\pi A}{Nm^* m_0} \int_0^{\frac{\pi}{2}} d\theta \sin^3\theta \cos\theta \int_0^\infty dp_0 p_0^5 \left\{\left(\frac{m^*}{m_0}\right) p_0^2 + 2m^* \chi\right\} \exp\left[-\frac{p_0^2}{2m_0 k_B T_e} - \frac{\chi}{k_B T_e}\right] \\ &\Rightarrow MTE = k_B T_e \left[\frac{3k_B T_e + \chi}{2k_B T_e + \chi}\right] \end{aligned}$$

The integral above for N may also be evaluated in cylindrical co-ordinates and thus separately over the transverse and longitudinal vacuum momenta, respectively, to give emitted electron distributions for PEA as a function of their longitudinal (E_z) and transverse (E_T) vacuum energies:

$$\begin{aligned} N(E_z) &= C k_B T_e \sqrt{E_z} \{E_z + \chi + k_B T_e\} \exp\left[-\frac{(E_z + \chi)}{k_B T_e}\right] \end{aligned}$$

and

$$N(E_T) = C k_B T_e \{E_T + \chi + k_B T_e\} \exp\left[-\frac{(E_T + \chi)}{k_B T_e}\right]$$

where C is a constant.

ii) Negative Electron Affinity

For a negative electron affinity (NEA) photocathode, the minimum of the emitting band is above the vacuum level, implying that $E = E_0 - |\chi|$, so that the momentum-space energy mapping is

$$p^2 = \left(\frac{m^*}{m_0}\right) p_0^2 - 2m^* |\chi|.$$

Hence, the three-dimensional non-degenerate electron distribution in the emitting bulk band can be written in vacuum momentum space as $\left\{\left(\frac{m^*}{m_0}\right) p_0^2 - 2m^* |\chi|\right\} \exp\left[-\frac{p_0^2}{2m_0 k_B T_e} + \frac{|\chi|}{k_B T_e}\right]$ for the interval p_0 to $p_0 + dp_0$ and $p_0 \geq \sqrt{2m_0 |\chi|}$. The number of emitted electrons is then given by

N

$$\begin{aligned}
&= 2\pi A \int_0^{\frac{\pi}{2}} d\theta \sin\theta \cos\theta \int_{\sqrt{2m_0\chi}}^{\infty} dp_0 p_0^2 \left(\frac{p_0}{m^*}\right) \left\{ \left(\frac{m^*}{m_0}\right) p_0^2 \right. \\
&\quad \left. - 2m^*|\chi| \right\} \exp \left[-\frac{p_0^2}{2m_0k_B T_e} + \frac{|\chi|}{k_B T_e} \right] \\
&= \pi A (2m_0k_B T_e)^2 [2k_B T_e + |\chi|]
\end{aligned}$$

As a result, in terms of T_e and χ , the barrier emission QE of the NEA FC process is of the form

$$QE \propto (k_B T_e)^2 [2k_B T_e + |\chi|]$$

Similarly, the MTE is again readily evaluated as for the PEA case using

$$\begin{aligned}
MTE &= \frac{\pi A}{Nm^*m_0} \int_0^{\frac{\pi}{2}} d\theta \sin^3\theta \cos\theta \\
&\quad \times \int_{\sqrt{2m_0|\chi|}}^{\infty} dp_0 p_0^5 \left\{ \left(\frac{m^*}{m_0}\right) p_0^2 \right. \\
&\quad \left. - 2m^*|\chi| \right\} \exp \left[-\frac{p_0^2}{2m_0k_B T_e} \right. \\
&\quad \left. + \frac{|\chi|}{k_B T_e} \right] \\
\Rightarrow MTE &= \frac{|\chi|}{2} + k_B T_e \left[\frac{3k_B T_e + |\chi|}{2k_B T_e + |\chi|} \right]
\end{aligned}$$

Clearly, as $\chi \rightarrow 0$, the evaluated MTEs for both the PEA and NEA cases equal $\frac{3}{2}k_B T_e$ and the QE values also converge to the same value.

Again, the integral above for N may be evaluated in cylindrical vacuum momentum co-ordinates to give emitted electron distributions for NEA as a function of their longitudinal (E_z) and transverse (E_T) vacuum energies:

$$N(E_z \leq |\chi|) = C(k_B T_e)^2 \sqrt{E_z}$$

$$\begin{aligned}
N(E_z > |\chi|) &= Ck_B T_e \sqrt{E_z} \{E_z - |\chi| \\
&\quad + k_B T_e\} \exp \left[-\frac{(E_z - |\chi|)}{k_B T_e} \right]
\end{aligned}$$

and

$$N(E_T \leq |\chi|) = C(k_B T_e)^2$$

$$\begin{aligned}
N(E_T > |\chi|) &= Ck_B T_e \{E_T - |\chi| \\
&\quad + k_B T_e\} \exp \left[-\frac{(E_T - |\chi|)}{k_B T_e} \right]
\end{aligned}$$

where C is a constant.

-
- [1] R. Xiang and J. Schaber, "Review of recent progress on advanced photocathodes for superconducting RF gun," *Micromachines*, vol. 13, p. 1241, 2022.
 - [2] D. Dowell et. al., "First operation of a photocathode radio frequency gun injector at high duty factor," *Appl. Phys. Lett.*, vol. 63, p. 2035, 1993.
 - [3] P. Michelato, "Photocathodes for RF photoinjector," *Nucl. Inst. & Meth. A*, vol. 393, p. 455, 1997.
 - [4] T. Vecchione, I. Ben-Zvi, D. Dowell, J. Feng, T. Rao, J. Smedley, W. Wan, and H. Padmore, "A low emittance and high efficiency visible light photocathode for high brightness accelerator-based X-ray light sources," *Appl. Phys. Lett.*, vol. 99, p. 034103, 2011.
 - [5] S. Quan et. al., "Stable operation of the DC-SRF photoinjector," *Nucl. Instrum. Meth. A*, vol. 798, p. 117, 2015.
 - [6] P. Musumeci et al., "Advances in bright electron sources," *Nucl. Inst. & Meth. A*, vol. 907, p. 209.
 - [7] E. Wang et al., "Long lifetime bialkali photocathodes operating in high gradient superconducting radio frequency gun," *Sci. Rep.*, vol. 11, p. 1, 2021.
 - [8] P. Emma et al., "First lasing and operation of an Angstrom-wavelength free electron laser," *Nat. Photonics*, vol. 4, p. 641, 2019.
 - [9] G. Sciani and R. J. D. Miller, "Femtosecond electron diffraction: Heralding the era of atomically resolved dynamics," *Rep. Prog. Phys.*, vol. 74, p. 096101, 2005.
 - [10] J. Hastings, F. Rudakov, D. Dowell, J. Schmerge, J. Cardoza, J. Castro, S. Gierman, H. Loos, and P. M. Weber, "Ultrafast time-resolved electron diffraction with megavolt electron beams," *Appl. Phys. Lett.*, vol. 89, p. 184109, 2006.
 - [11] R. Li, C. Tang, Y. Du, W. Huang, Q. Du, J. Shi, L. Yan, and X. Wang, "Experimental demonstration of high quality MeV ultrafast electron diffraction," *Rev. Sci. Instrum.*, vol. 80, p. 083303, 2009.
 - [12] P. Musumeci, J. Moody, C. Scoby, M. Gutierrez, H. Bender, and N. Wilcox, "High quality single shot diffraction patterns using ultrashort megaelectron volt beams from a

- radio frequency photoinjector," *Rev. Sci. Instrum.*, vol. 81, p. 013306, 2010.
- [13] S. Weathersby et al., "Mega-electron-volt ultrafast electron diffraction at SLAC National Accelerator Laboratory," *Rev. Sci. Instrum.*, vol. 86, p. 073702, 2015.
- [14] D. Dowell et al., "Cathode R&D for future light sources," *Nucl. Inst. & Meth. A*, vol. 622, pp. 685-697, 2010.
- [15] N. Terunuma et al., "Improvement of an S-band RF gun with a Cs₂Te photocathode for the KEK-ATF," *Nucl. Inst. & Meth. A*, vol. 613, p. 1, 2010.
- [16] E. Prat, S. Bettoni, H.-H. Braun, R. Ganter, and T. Schietinger, "Measurements of copper and cesium telluride cathodes in a radio-frequency photoinjector," *Phys. Rev. STAB*, vol. 18, p. 043401, 2015.
- [17] F. Zhou et al., "Commissioning of the SLAC Linac Coherent Light source II electron source," *Phys. Rev. Accel. & Beams*, vol. 24, p. 073401, 2021.
- [18] W. Spicer, "Photoemissive, photoconductive, and optical absorption studies of alkali-antimony compounds," *Phys. Rev.*, vol. 112, p. 114, 1958.
- [19] L. Cultrera, I. Bazarov, A. Bartnik, B. Dunham, S. Karkare, R. Merluzzi, and M. Nichols, "Thermal emittance and response time of a cesium antimonide photocathode," *Appl. Phys. Lett.*, vol. 99, p. 152110, 2011.
- [20] L. Cultrera, S. Karkare, H. Lee, X. Liu, I. Bazarov, and B. Dunham, "Cold electron beams from cryocooled, alkali antimonide photocathodes," *Phys. Rev. STAB*, vol. 18, p. 113401, 2015.
- [21] A. Galdi, J. Balajka, W. DeBenedetti, L. Cultrera, I. V. Bazarov, M. Hines, and J. M. Maxson, "Reduction of surface roughness emittance of Cs₃Sb photocathodes grown via codeposition on single crystal substrates," *Appl. Phys. Lett.*, vol. 118, p. 244101, 2021.
- [22] C. T. Parzyck et al., "Single-crystal alkali antimonide photocathodes: High efficiency in the ultrathin limit," *Phys. Rev. Lett.*, vol. 128, p. 114801, 2022.
- [23] I. Bazarov, L. Cultrera, A. Bartnik, B. Dunham, S. Karkare, Y. Li, X. Liu, J. Maxson, and W. Roussel, "Thermal emittance measurements of a cesium potassium antimonide photocathode," *Appl. Phys. Lett.*, vol. 98, p. 224101, 2011.
- [24] J. Maxson, L. Cultrera, C. Gulliford, and I. Bazarov, "Measurement of the tradeoff between intrinsic emittance and quantum efficiency from a NaKSb photocathode near threshold," *Appl. Phys. Lett.*, vol. 106, p. 234102, 2015.
- [25] D. Pierce and F. Meier, "Photoemission of spin-polarized electrons from GaAs," *Phys. Rev. B*, vol. 13, p. 5484, 1976.
- [26] D. Pierce, R. Celotta, G. Wang, W. Unertl, A. Galejs, and C. Kuyatt, "The GaAs spin polarized electron source," *Rev. Sci. Instrum.*, vol. 51, pp. 478-499, 1980.
- [27] J. Kirschner, H. P. Oepen, and H. Ibach, "Energy- and spin-analysis of polarized photoelectrons from NEA GaAs," *Appl. Phys. A*, vol. 30, p. 177, 1983.
- [28] J. Bae, L. Cultrera, P. Digiacomio, and I. Bazarov, "Rugged spin-polarized electron sources based on negative electron affinity GaAs photocathode with robust Cs₂Te coating," *Appl. Phys. Lett.*, vol. 112, p. 154101, 2018.
- [29] S. Levenson, M. Andorf, B. Dickensheets, I. Bazarov, A. Galdi, J. Encomendero, V. Protasenko, D. Jena, H. Xing, and J. M. Maxson, "Measurement of spin-polarized photoemission from wurtzite and zinc blende gallium nitride photocathodes," *Appl. Phys. Lett.*, vol. 125, p. 034107, 2024.
- [30] N. Yamamoto et al., "High brightness and high polarization electron source using transmission photocathode with GaAs-GaAsP superlattice layers," *J. Appl. Phys.*, vol. 103, p. 964905, 2008.
- [31] P. Adderley et al., "An overview of how parity violating electron scattering experiments are performed at CEBAF," *Nucl. Instrum. Methods Phys. Res. A*, vol. 1046, p. 167710, 2023.
- [32] A. Deur et al., "Measurement of the nucleon spin structure functions for $0.01 < Q^2 < 1\text{-GeV}^2$ using CLAS," arXiv:2409.08365 [nuc-ex], 2024.
- [33] M. Suzuki et al., "Real time magnetic imaging by spin-polarized low energy electron microscopy with highly spin-polarized and high brightness electron gun," *Appl. Phys. Express*, vol. 3, p. 026601, 2010.
- [34] N. Rougemaille and A. Schmid, "Magnetic imaging with spin-polarized low energy electron microscopy," *Eur. J. Appl. Phys.*, vol. 50, p. 20101, 2010.

- [35] M. Kuwahara et al., "Coherence of a spin-polarized electron beam emitted from a semiconductor photocathode in a transmission electron microscope," *Appl. Phys. Lett.*, vol. 105, p. 193101, 2014.
- [36] W. Spicer, "Negative affinity 3-5 photocathodes: Their physics and technology," *Appl. Phys.*, vol. 12, p. 115, 1977.
- [37] A. Baum, W. Spicer, R. Pease, K. Costello, and V. W. Aebi, "Negative electron affinity photocathodes as high-performance electron sources – Part 2: Energy spectrum measurements," *Proc. SPIE*, vol. 2550, p. 189, 1995.
- [38] I. Bazarov, B. M. Dunham, Y. Li, X. Liu, D. Ouzounov, C. Sinclair, F. Hannon, and T. Miyajima, "Thermal emittance and response time measurements of negative electron affinity photocathodes," *J. Appl. Phys.*, vol. 103, p. 054901, 2008.
- [39] Y. Honda, S. Matsuba, X. Jin, T. Miyajima, M. Yamamoto, T. Uchiyama, M. Kuwahara, and Y. Takeda, "Temporal response measurements of GaAs-based photocathodes," *Jpn. J. Appl. Phys.*, vol. 2013, p. 086401, 2013.
- [40] N. Chanlek, J. Herbert, R. Jones, L. Jones, K. Middleman, and B. Militsyn, "High stability of negative electron affinity gallium arsenide photocathodes activated with Cs and NF_3 ," *J. Phys. D: Appl. Phys.*, vol. 48, p. 375102, 2015.
- [41] S. Uchiyama, Y. Takagi, M. Niigaki, H. Kan, and H. Kondoh, "GaN-based photocathodes with extremely high quantum efficiency," *Appl. Phys. Lett.*, vol. 86, p. 103511, 2005.
- [42] I. Bazarov, B. Dunham, X. Liu, M. Virgo, M. Dadiran, F. Hannon, and H. Sayed, "Thermal emittance and response time measurements of a GaN photocathode," *J. Appl. Phys.*, vol. 105, p. 083715, 2009.
- [43] N. Chanlek, J. Herbert, R. Jones, L. Jones, K. Middleman, and B.L. Militsyn, "The degradation of quantum efficiency in negative electron affinity GaAs photocathodes under gas pressure," *Appl. Phys.*, vol. 47, p. 055110, 2014.
- [44] L. Jones, H. Scheibler, S. Kosolobov, A. Terekhov, B. Militsyn, and T. Noakes, "Non-monotonic behaviour in the mean transverse energy of electrons emitted from a reflection-mode p-GaAs(Cs,O) photocathode during its QE degradation through oxygen exposure," *J. Phys. D: Appl. Phys.*, vol. 54, p. 205301, 2021.
- [45] W.E. Spicer, A. Herrera-Gomez, Modern theory and applications of photocathodes, in: *Proceedings of the SPIE*, vol. 2022, K. J. Kaufmann (Ed.), Photodetectors and power meters, pp. 18–35.
- [46] D. Dowell and J. Schmerge, "Quantum efficiency and thermal emittance of metal photocathodes," *Phys. Rev. St Accel. Beams*, vol. 12, p. 074201, 2009; Erratum, *Phys. Rev. St Accel. Beams* **12**, 119901 (2009).
- [47] T. Vecchione, D. Dowell, W. Wan, J. Feng, and H. Padmore, "Quantum efficiency and transverse momentum from metals," *Proceedings of FEL2013*, New York, NY, 2013 (JACoW, Geneva, Switzerland, 2013), p. 424.
- [48] S. Karkare, D. Dimitrov, W. Schaff, L. Cultrera, A. Bartnik, X. Liu, E. Sawyer, T. Esposito, and I. Bazarov, "Monte Carlo charge transport and photoemission from negative electron affinity GaAs photocathodes," *J. Appl. Phys.*, vol. 113, p. 104904, 2013; Erratum, *J. Appl. Phys.*, vol. 117, p. 109901, 2015.
- [49] J. Marini, L. Bell, and F. Shahedipour-Sandvik, "Monte Carlo simulation of III-nitride photocathodes," *J. Appl. Phys.*, vol. 123, p. 124502, 2018.
- [50] F. Himpsel, "Angle-resolved measurements of the photoemission of electrons in the study of solids," *Adv. Phys.*, vol. 32, p. 1, 1983.
- [51] G. Vergara, A. Herrera-Gomez, and W. Spicer, "Electron transverse energy distribution in GaAs negative electron affinity cathodes: Calculations compared to experiments," *J. Appl. Phys.*, vol. 80, p. 1809, 1996.
- [52] R. Bell, *Negative Electron Affinity Devices*, Oxford: Clarendon Press, 1973.
- [53] V. Bakin, A. Pakhnevich, S. Kosolobov, H. Scheibler, A. Jaroshevich, and A. Terekhov, "Refraction of thermalized electrons emitted ballistically into vacuum from p + -GaAs-(Cs,O)," *JETP Lett.*, vol. 77, p. 167, 2003.
- [54] B. Rickman, J. Berger, A. Nicholls, and W. A. Schroeder, "Intrinsic electron beam emittance from metal photocathodes: The effect of the electron effective mass," *Phys. Rev. Lett.*, vol.

- 111, p. 237401, 2013; Erratum: Phys. Rev. Lett., vol. 113, p. 239904, 2014.
- [55] W. Schroeder and G. Adhikari, "Evaluation of photocathode emission properties in an electron gun: One-step photoemission from bulk-band to vacuum states," *New J. Phys.*, vol. 21, p. 033040, 2019.
- [56] H. Qian, C. Li, Y. Du, L. Yan, J. Hua, W. Huang, and C. X. Tang, "Experimental investigation of thermal emittance components of copper photocathode," *Phys. Rev. St Accel. Beams*, vol. 15, p. 040102, 2012.
- [57] S. Karkare and I. Bazarov, "Effects of surface nonuniformities on the mean transverse energy from photocathodes," *Phys. Rev. Applied*, vol. 4, p. 024015, 2015.
- [58] D. Bradley, M. B. Allenson, and B. Holeman, "The transverse energy of electrons emitted from GaAs photocathodes," *J. Phys. D: Appl. Phys.*, vol. 10, p. 111, 1977.
- [59] J. Franck, "Elementary processes of photochemical reactions," *Trans. Farad. Soc.*, vol. 21, p. 536, 1926.
- [60] E. Condon, "A theory of intensity distribution in band systems," *Phys. Rev.*, vol. 28, p. 1182, 1926.
- [61] J. Rameau, J. Smedley, E. Muller, T. Kidd, and P.D. Johnson, "Properties of hydrogen terminated diamond as a photocathode," *Phys. Rev. Lett.*, vol. 106, p. 137602, 2011.
- [62] N. Tandon and J. Albrecht, "Electron-phonon coupling and associated scattering rates in diamond," *Diam. Relat. Mater.*, vol. 56, p. 1, 2015.
- [63] D. Orlov, V. Andreev, and A. S. Terekhov, "'Elastic and inelastic tunneling of photoelectrons from the dimensional quantization band a p + -GaAs-(Cs,O) interface into vacuum," *JETP Lett.*, vol. 71, p. 151, 2000.
- [64] L. James and J. Moll, "Transport properties of GaAs obtained from photoemission measurements," *Phys. Rev.*, vol. 183, p. 740, 1969.
- [65] J. Nangoi, T. Arias, S. Karkare, H. Padmore, and W. A. Schroeder, "The role of electron-phonon scattering in transverse momentum conservation in PbTe(111) photocathodes," in *Proceedings of the 9th International Particle Accelerator Conference (IPAC'18)*, April 29-May 4, 2018, Vancouver, British Columbia, Canada, pp. 1414-1416 (JACOW Publishing, Geneva, Switzerland).
- [66] J. Blakemore, "Semiconducting and other major properties of gallium arsenide," *J. Appl. Phys.*, vol. 53, pp. R123-R181, 1982.
- [67] J. F. Muth, J. D. Brown, M. A. L. Johnson, R. M. K. Z. Yu, J. W. C. Jr., and J. F. Schetzina, "Absorption Coefficient and Refractive Index of GaN, AlN, and AlGa_N Alloys," *Materials Research Society Internet Journal of Nitride Semiconductor Research*, vol. 4, no. S1, 2014.
- [68] C. M. Balkas, Z. Sitar, L. Bergman, I. Shmagin, J. F. Muth, R. Kolbas, R. J. Nemanich, and R. Davis, "Growth and Characterization of GaN single crystals," *Journal of Crystal Growth*, vol. 208, pp. 100-106, 1999.
- [69] L. Angeloni, S. Baryshev, M. Mühle, and W. A. Schroeder, "Spectral Emission Properties of a Nitrogen-doped Diamond(001) Photocathode: Hot Electron Transport and Transverse Momentum Filtering," *Phys. Rev. B*, vol. 107, p. 165105, 2023.
- [70] G.D. Mahan, *Many-Particle Physics 2nd ed.*, New York: Plenum Press, 1990.
- [71] J. Devreese, R. Lerner, and G. L. Trigg, "Polarons," in *Encyclopedia of Physics vol. 2 (3rd edition)*, Weinheim: Wiley-VCH, 2005, pp. 2004-2027.
- [72] K. Ishizaka et al., "Temperature-dependent localized excitations of doped carriers in superconducting diamond," *Phys. Rev. Lett.*, vol. 100, p. 166402, 2008.
- [73] K. Seeger, "Semiconductor Physics – An Introduction," in *Springer Series in Solid-State Sciences*, 40 (1989).
- [74] M. E. Mora-Ramos, F. J. Rodriguez, and L. Quiroga, "Polarons in Wurtzite Nitride Semiconductors," *Solid State Communications*, vol. 109, no. 12, pp. 767-772, 1999.
- [75] L. Jones, H. Scheibler, D. Gorshkov, A. S. Terekhov, B. Militsyn, and T. C. Q. Noakes, "Evolution of the transverse and longitudinal energy distributions of electrons emitted from a GaAsP photocathode as a function of its degradation state," *J. Appl. Phys.*, vol. 121, p. 225703, 2017.
- [76] L. Jones, D. Juarez-Lopez, H. Scheibler, A. Terekhov, B. Militsyn, C. Welsch, and T. Noakes, "The measurement of photocathode transverse energy distribution curves (TEDCs) using the transverse energy spread

- spectrometer (TESS) experimental system," *Rev. Sci. Instrum.*, vol. 93, p. 113314, 2022.
- [77] L. Devlin, L. Jones, T. Noakes, C. Welsch, and B. Militsyn, "Measurement of the longitudinal energy distribution of electrons in low energy beams using electrostatic elements," *Rev. Sci. Instrum.*, vol. 89, p. 083305, 2018.
- [78] M. Sotoodeh, A. Khalid, and A. A. Rezazadeh, "Empirical low-field mobility model for III-V compounds applicable in device simulation codes," *J. Appl. Phys.*, vol. 87, p. 2890, 2000.
- [79] S. Svensson, J. Kanski, T. Andersson, and P.-O. Nilsson, "Photoemission studies of the band bending on MBE-grown GaAs(001)," *J. Vac. Sci. Technol.*, vol. 2, p. 235, 1984.
- [80] J. Kash, J. Tsang, and J. Hvam, "Subpicosecond time-resolved Raman spectroscopy of LO phonons in GaAs," *Phys. Rev. Lett.*, vol. 54, p. 2151, 1985.
- [81] "kymatech.com".
- [82] O. Ambacher et al., "Two dimensional electron gases induced by spontaneous and piezoelectric polarizations in undoped and doped AlGaIn/GaN heterostructures," *Journal of Applied Physics*, vol. 87, pp. 334-344, 2000.
- [83] M. J. Murphy, K. Chu, H. Wu, W. Yeo, W. J. Schaff, O. Ambacher, J. Smart, J. R. Shealy, L. F. Eastman, and T. J. Eustis, "Molecular beam epitaxial growth of normal and inverted two-dimensional electron gases in AlGaIn/GaN based heterostructures," *Journal of Vacuum Science & Technology B*, vol. 17, pp. 1252-1254, 1999.
- [84] C. Fall, N. Binggeli, and A. Baldereschi, "Deriving accurate work functions from thin-slab calculations," *J. Phys.: Cond. Matter*, vol. 11, p. 2689, 1999.
- [85] L. Cultrera, E. Rocco, F. S.-. Sandvik, L. D. Bell, J. K. Bae, I. V. Bazarov, P. Saha, S. Karkare, and A. Arjunan, "A photoemission characterization of N-polar III-nitride photocathodes as candidate bright electron beam sources for accelerator physics," *J. Appl. Phys.*, vol. 131, p. 124902, 2022.
- [86] A. Udabe, I. Baraia-Etxaburu, and D. G. Diez, "Gallium Nitride Power Devices: A State of the Art Review," *IEEE Access*, vol. 11, pp. 48627-48647, 2023.
- [87] M. Goano, E. Bellotti, E. Ghillino, G. Ghione, and K. Brennan, "Band structure nonlocal pseudopotential calculation of the III-nitride wurtzite phase materials system. Part I. Binary compounds GaN, AlN, and InN," *J. Appl. Phys.*, vol. 88, p. 6467, 2000.
- [88] T. Hashizume, "Effects of Mg accumulation on chemical and electronic properties of Mg-doped p-type GaN surface," *Journal of Applied Physics*, vol. 94, pp. 431-436, 2003.
- [89] J. Kolnik, I. Oguzman, K. Brennan, R. Wang, P. Ruden, and Y. Wang, "Electronic transport studies of bulk zincblende and wurtzite phases of GaN based on an ensemble Monte Carlo calculation including a full zone band structure," *J. Appl. Phys.*, vol. 78, p. 1033, 1995.
- [90] U. Bhapkar and M. S. Shur, "Monte Carlo calculation of velocity-field characteristics of wurtzite GaN," *J. Appl. Phys.*, vol. 82, p. 4, 1997.
- [91] J. Khurgin, Y. Ding, and D. Jena, "Hot phonon effect on electron velocity saturation in GaN: A second look," *Appl. Phys. Lett.*, vol. 91, p. 252104, 2007.
- [92] K. Tsen, J. Kiang, D. Ferry, and H. Morkoc, "Subpicosecond time-resolved Raman studies of LO phonons in GaN: Dependence on photoexcited carrier density," *Appl. Phys. Lett.*, vol. 89, p. 112111, 2006.
- [93] V. Yu. et al., "Phonon dispersion and Raman scattering in hexagonal GaN and AlN," *Phys. Rev. B*, vol. 58, p. 12899, 1998.
- [94] B. Santic, "On the hole effective mass and free hole statistics in wurtzite GaN," *Semiconductor Science and Technology*, vol. 18, p. 219, 2003.
- [95] G. Adhikari, P. Riley, and W.A. Schroeder, "Spectral characterization of a Rh(110) photocathode: Band structure interpretation," *AIP Advances*, vol. 9, p. 06305, 2019.
- [96] L. Angeloni, I.-J. Shan, and W. A. Schroeder, "Sub-threshold ultrafast one-photon photoemission from a Cu(111) photocathode," *AIP Advances*, vol. 12, p. 105129, 2022.
- [97] P. Kozodoy, H. Xing, S. P. DenBaars, U. K. Mishra, A. Saxler, R. Perrin, S. Elhamri, and W. C. Mitchel, "Heavy Doping Effects in Mg-doped GaN," *Journal of Applied Physics*, vol. 87, pp. 1832-1835, 2000.
- [98] W. Gotz, N. Johnson, C. Chen, H. Liu, C. Kuo, and W. Imler, "Activation energies of Si donors in GaN," *Appl. Phys. Lett.*, vol. 68, p. 3144, 1996.

- [99] C. Order, S. Einfeldt, S. Figge, and D. Hommel, "Temperature dependence of the thermal expansion of GaN," *Phys. Rev. B*, vol. 72, p. 085218, 2005.
- [100] K. Tsen, D. Ferry, A. Botchkarev, B. Sverdlov, A. Salvador, and H. Morkoc, "Direct measurements of electron-longitudinal optical phonon scattering rates in wurtzite GaN," *Appl. Phys. Lett.*, vol. 71, p. 1852, 1997.
- [101] S. Karkare and I. Bazarov, "Effect of nanoscale surface roughness on transverse energy spread from GaAs photocathodes," *Appl. Phys. Lett.*, vol. 98, p. 094104, 2011.
- [102] A. Zhuravlev, D. M. Kazantsev, V. Khoroshilov, A. Kozhukhov, and V. L. Alperovich, "Photoemission properties of flat and rough GaAs surfaces with cesium and oxygen layers," in *IOP Conf. Series: Journal of Physics: Conf. Series* 993, 012007 (2018).
- [103] J. Biswas, J. Cen, M. Gaowei, O. Rahman, X. T. W. Liu, and E. Wang, "Revisiting heat treatment and surface activation of GaAs photocathodes: In situ studies using scanning tunneling microscopy and photoelectron spectroscopy," *J. Appl. Phys.*, vol. 128, p. 045308, 2020.
- [104] Z. Zhang and C. Tang, "photocathode, Analytical study on emittance growth caused by roughness of a metallic," *Phys. Rev. ST Accel. Beams*, vol. 18, no. p. 053401, 2015.
- [105] C. Cocchi, S. Mistry, M. Schmeißer, R. Amador, J. Kühn, and T. Kamps, "Electronic structure and core electron fingerprints of caesium-based multi-alkali antimonides for ultra-bright electron sources," *Scientific Reports*, vol. 9, p. 18276, 2019.
- [106] P. Gupta, L. Cultrera, and I. Bazarov, "Monte Carlo simulations of electron photoemission from cesium antimonide," *J. Appl. Phys.*, vol. 121, p. 215702, 2017.